[Summary of Doctoral Dissertation]

Structure Design in Micro/Nano Scale of Sn-Based Phase Change Materials for Thermal Energy Storage

ZHU Shilei

1. Background and Objectives

Phase change or phase transition, as one of the most common phenomena that occurs every second in our planet, was used to describe transitions between solid, liquid, gaseous states as well as plasma of matters. Phase change materials (PCMs) are recognized as the materials that use phase transitions to achieve certain designed functions. Using latent heat in PCMs is one of the most efficient ways of storing thermal energy and it has received wide attention in decades. Among PCMs based on different phase change processes, solid-liquid PCMs are the most studied and used storage medium of thermal energy due to the high enthalpy of fusion and small volume expansion. Various types of solid-liquid PCMs were developed including both organics compounds (e.g., paraffin waxes, fatty acids, esters and other organic compounds) and inorganics compounds (e.g., salt hydrates, molten salts, metals and alloys). However, the biggest historical drawback of using conventional PCMs, like the low thermal conductivity of organic materials and inorganic salts, large volume changes of inorganic salts during melting ,and high corrosion from inorganic salts and metals.[1-5] Those give limitations for their wider applications.[3, 6]

Metals and their alloys can overcome the problems existing in organic compounds and inorganic salts as mentioned above. Low melting point metals are promising materials that can be used as PCM for heat storage and thermal management in wider working conditions.[4, 6, 7] Due to the high thermal conductivity, the metallic heat storage media shows rapid thermal energy transfer.[8] In addition, the high density of the metals also contributes to the high volumetric density of heat storage.[3] Based on these advantages, the low melting point metals can be applied in the thermal energy storage system in concentrated solar power (CSP) station.[9, 10] It also could be used for chip cooling in USB flash memory,[11] smartphones[12] and other high power density devices.[13, 14]

However, as a high performance PCM in thermal energy storage and management, the low melting point metals or alloys still in demand of efforts to be modified for practical applications. First, due to the corrosive characteristics of metals in liquid state, the compatibility between low melting point metal PCM and its container should be guaranteed. The bad compatibility between liquid metals and container, seriously limited their applications. Moreover, the sintering of liquid metal particles in low melting point metal PCMs may lead to the changes in as-designed structure or morphology during operation, deteriorating their sustainable usage in the form of nanofluids or slurry.[15] Therefore, the structure design for encapsulating in micro or nano-sized low melting point metal PCMs in need for improving their utility.

The aims of this dissertation are to explore various synthetic methods, to create unique micro/nanostructures, thus, to make the best use of the high thermal conductivity of low melting

point metal PCMs, isolate them from outside environment for protection and also seek the novel methods for the further morphology control of related PCMs. Silica (SiO_2) and alumina (Al_2O_3) were chosen as the encapsulation materials due to their good physical and chemical stability. [16] Until now, only a few examples have been reported to achieve using SiO_2 and Al_2O_3 to coat low-melting-point metal for thermal energy storage[17]. Compared to them, in this dissertation, more facile and more customized methods were used, and the PCMs with unique structures named Sn NPs@p-SiO_2 and Sn@Al_2O_3 with good thermal cyclic stability were fabricated. In the case of using SiO_2 to encapsulate Sn NPs, a novel transformation from Sn@SiO_2 core-shell NPs to Sn@SiO_2 yolk-shell NPs and SnO_2@SiO_2 hollow NPs were observed, based on which the nanostructure control via liquid metal diffusion was first time realized.

2. Materials and Methods

2.1 Synthesis of Sn NPs@p-SiO_2

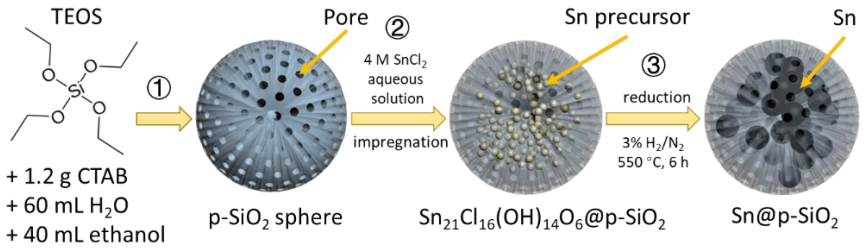

Scheme 1. Preparation of Sn NPs@p-SiO_2. Step 1: Synthesis of p-SiO_2 spheres as structure matrix; Step 2: Impregnation of the Sn precursor; Step 3: Reduction of the Sn precursor inside the SiO_2 matrix to obtain Sn NPs embedded into p-SiO_2.

Porous p-SiO_2 spheres were first prepared by the hydrolysis and condensation of TEOS triggered by ammonia in the mixture of ethanol and H_2O with the existence of CTAB. The obtained p-SiO_2 spheres were purified and vacuum-dried overnight then used as matrix and dispersed in $SnCl_2$ solution for loading Sn precursor. After removing the unabsorbed Sn precursor by purification and drying in vacuum, the powder was reduced by thermal annealing in a mixed H_2/N_2 (3:97) gas flow at 550°C for 6 h in a tube furnace. Finally, Sn NPs@p-SiO_2 was obtained as a black powder.

2.2 Synthesis of Sn@Al_2O_3

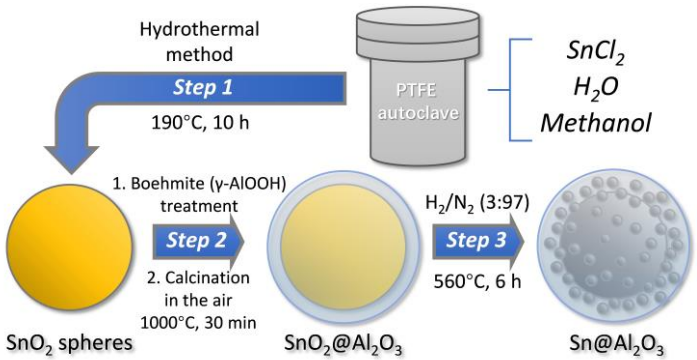

Scheme 2. Synthesis process of Sn@Al_2O_3 spheres.

First, SnO_2 spheres were prepared by a solvothermal method from $SnCl_2$ precursor in a Teflon-lined stainless-steel autoclave. Then, the SnO_2 spheres were dispersed in a pre-prepared boehmite solution and refluxed for 12 h. After purification with deionized water and 1-propanol, and drying in vacuum, the powder was calcined at 1000°C in the air in a tube furnace for 30 min, and finally reduced by a mixed H_2/N_2 (3:97) gas flow at 560 °C for 6 h. The final product, $Sn@Al_2O_3$, was obtained as a black powder.

2.3 Synthesis of $Sn@SiO_2$

The Sn NPs were synthesized using a well-developed hot-injection method. Developed method.[18] To encapsulate Sn NPs with uniform SiO_2 shell, a modified reversed micro-emulsion method was used. Sn nanoparticle-dispersed stock solution (in hexane) was mixed with polyethylene glycol mono-4-nonylphenyl ether and deionized water to make emulsion by sonication. Afterward, TEOS were added, and the hydrolysis and condensation of TEOS were triggered by injection of ammonia solution for making the SiO_2 encapsulation on Sn NPs. The thickness of SiO_2 shell can be easily tuned by changing the concentration of Sn nanoparticle-dispersed stock solution.

2.4 In-situ Transmission Electron Microscopy (TEM) Observation of the Transformation of $Sn@SiO_2$ Core-Shell NPs to Yolk-Shell NPs and Hollow NPs

In situ TEM observations were carried out using a dedicated 1000 kV JEM-1000K RS TEM (JEOL, Tokyo, Japan) operated at 1000 kV. A wire-type heating holder (JEOL, EM-Z081834SWHH, Tokyo, Japan) was used. The powder samples ($Sn@SiO_2$) were loaded on a tungsten wire and heated up to 300°C under vacuum. TEM images were recorded with a charge-coupled device with an exposure time of typically 0.5 s and 5 s. The electron beam current flux for strong electron beam condition was 37.3 $pA \cdot cm^{-2}$, and for weak electron beam condition was 2.7 $pA \cdot cm^{-2}$, as measured with a Faraday gauge.

3. Results and Discussion

3.1 Sn Nanoparticles Confined in Porous Silica Spheres for Enhanced Thermal Cyclic Stability

In this part (Chapter 2), Sn NPs@p-SiO_2 spheres with the diameter of *ca.* 400 nm was successfully synthesized. The size of Sn NPs distributed inside p-SiO_2 is *ca.* 30 nm in diameter. The structure of Sn NPs@p-SiO_2 was investigated by using TEM, X-ray diffraction (XRD), X-ray photoelectron spectroscopy (XPS) depth profile techniques. X-ray fluorescence spectrometry (XRF) was used to estimate the elemental composition. The results show that Sn NPs are uniformly embedded inside the p-SiO_2 spheres (Figure 1A). The formation mechanism of Sn NPs@p-SiO_2 was discussed, First, Sn precursors (main composition: $Sn_{21}Cl_{16}(OH)_{14}O_6$) are absorbed into p-$SiO_2$ spheres after the impregnation of the $SnCl_2$ precursor. Then, amorphous Sn precursor is formed after annealing at a temperature below 260°C. After that, crystal Sn oxides (SnO_x, x = 1, 2) form at *ca.* 330°C with a change in the pore structure of the p-SiO_2 spheres. Finally, SnO_x is reduced and Sn NPs are formed inside the p-SiO_2 spheres with the ability to further expand the pores inside the p-SiO_2 spheres (Figure 1B).

To investigate the stability of the separated distribution of Sn NPs inside p-SiO_2, 100 melt–freeze thermal cycles were performed in the 100–250°C range. The results show a good

long-term thermal stability and decreased melting temperature of Sn which is corresponding to the nanoscale characteristic (Figure 1C). No morphology changes were observed before and after cycling according to the TEM images.

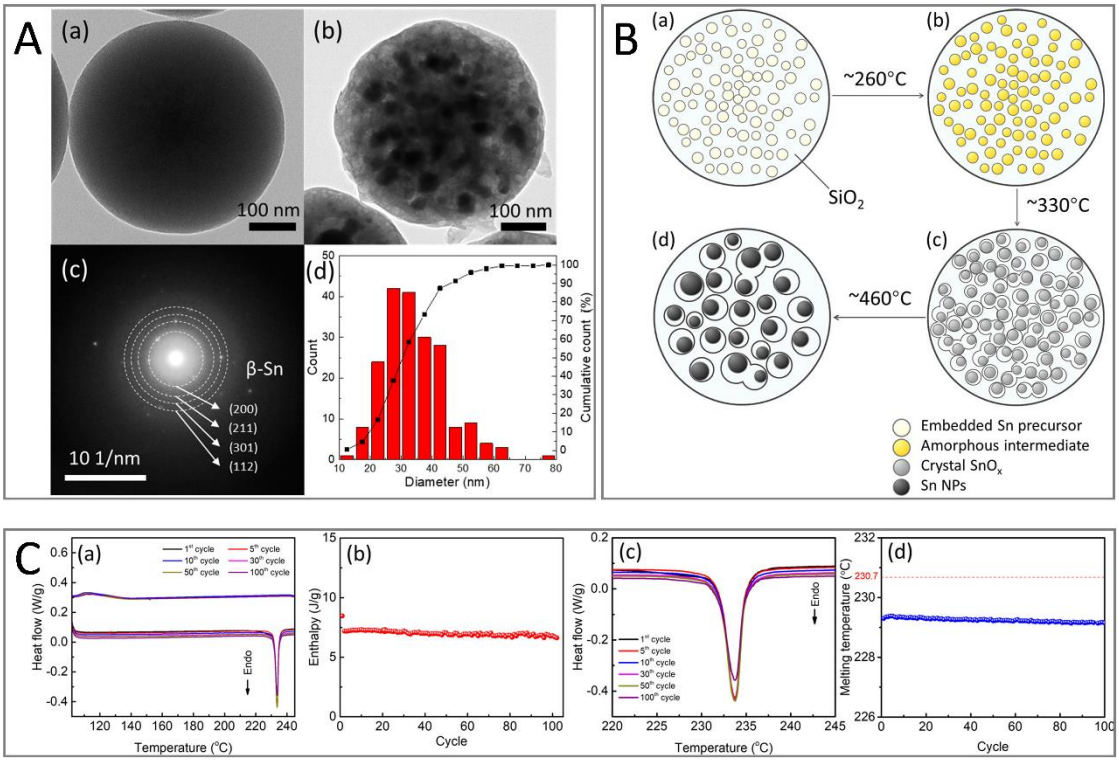

Figure 1. (A): (a, b) TEM images of (a) as-synthesized p-SiO_2 spheres and (b) Sn NPs@p-SiO_2. (c) SAED pattern of Sn NPs@p-SiO_2. (d) Size histogram of Sn NPs in p-SiO_2; (B): Illustration of the mechanism of Sn NPs@p-SiO_2 formation; (C): (a) DSC results for 100 melt–freeze cycles for Sn NPs@p-SiO_2. (b) Enthalpy of melting vs cycle number. (c) Enlarged DSC curves in the 220–245°C range during 100 cycles. (d) Melting temperature of Sn NPs confined into p-SiO_2 (blue spheres) at each cycle compared with the melting temperature of bulk Sn (red dashed line).

3.2 Size-Tunable Alumina-Encapsulated Sn-Based Phase Change Materials for Thermal Energy Storage

In this part (Chapter 3), Sn@Al_2O_3 was examined by TEM, scanning electron microscopy (SEM), energy-dispersive X-ray spectroscopy (EDS), and XRD, in which a big spherical Sn core (1–2 μm) and many small Sn spheres (50–250 nm) were encapsulated by a thick Al_2O_3 shell (100–700 nm) (Figure 2A). The obtained Sn@Al_2O_3 particles not only have high PCM content (92.37 wt %) but also show a stable thermal behavior and morphology during 100 melt–freeze cycles in the air atmosphere (Figure 2B, C).

To investigate the formation mechanism of Sn@Al_2O_3, the intermediate SnO_2@Al_2O_3 was checked by TEM, XRD, SEM, focused ion beam (FIB) cross-section imagine and XPS. It was found that the boehmite treatment, in which the penetration of aluminum species into SnO_2 spheres played an important role, was found to be responsible for the unique structure formation of final Sn@Al_2O_3. To test this finding above, the Sn@Al_2O_3 samples with different sizes from ~600 to ~60 nm were synthesized for comparison with Sn@Al_2O_3 obtained from the standard synthesis, showing a good control in size of Sn@Al_2O_3 (Figure 3). The understanding

of structure formation mechanism gives the possibilities of a new facile way for the synthesis of metal nanoparticles and particle-distributed nanostructures.

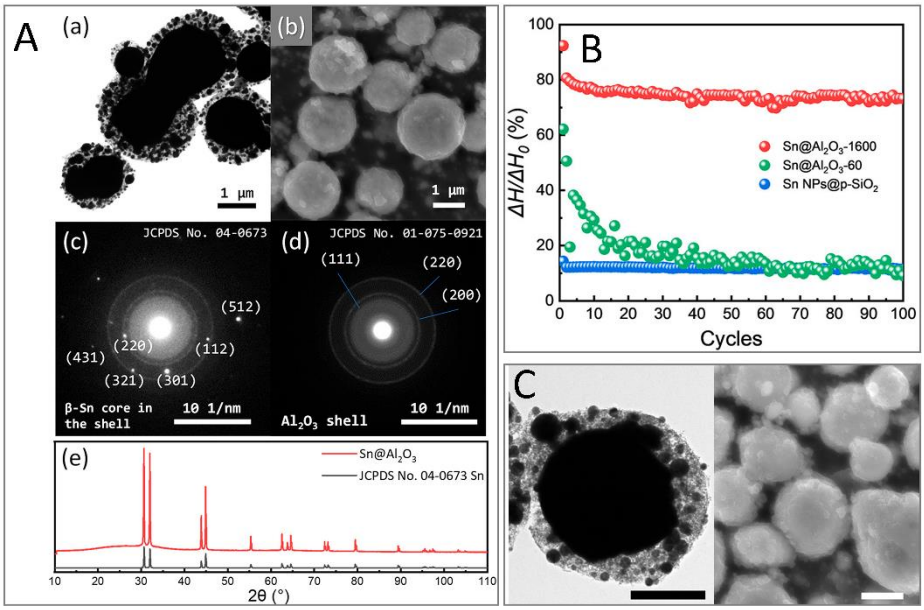

Figure 2. (A): TEM (a) and SEM (b) images of Sn@Al_2O_3 particles. SAED patterns of black cores inside shell of Sn@Al_2O_3 (c) and shell with light contrast (d). (e) XRD pattern of as-prepared Sn@Al_2O_3 particle powder; (B): Relative melting enthalpy in 100 melt–freeze cycles of Sn@Al_2O_3-1600 compared with bulk Sn ($\Delta H/\Delta H_0$) during melt–freeze cycles (red spheres) where ΔH and $\Delta H_0$are enthalpy of melting of Sn@Al_2O_3-1600 and that of bulk Sn, respectively. The relative melting enthalpies of Sn@Al_2O_3-60 and Sn NPs@p-SiO_2 are labeled with green and blue spheres, respectively; (C): TEM and SEM images of Sn@Al_2O_3-1600 after 100 melt–freeze cycles in the air.

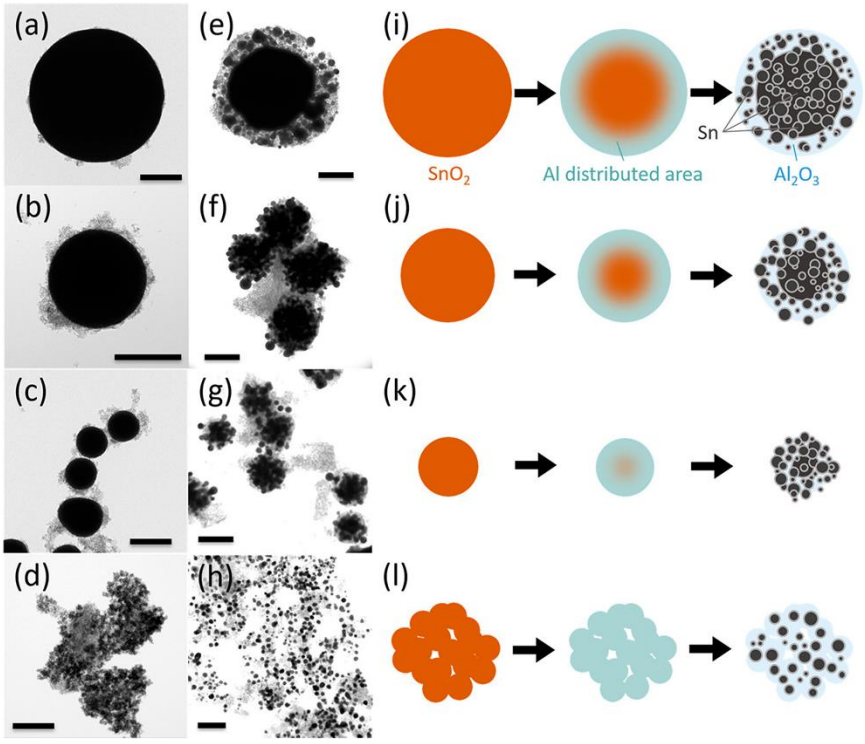

Figure 3. TEM images of (e–h) $Sn@Al_2O_3$ with different morphologies (e: $Sn@Al_2O_3$-1600; f: $Sn@Al_2O_3$-600; g: $Sn@Al_2O_3$-350; h: $Sn@Al_2O_3$-60) reduced from the corresponding (a–d) $SnO_2@Al_2O_3$ (a: $SnO_2@Al_2O_3$-1600; b: $SnO_2@Al_2O_3$-600; c: $SnO_2@Al_2O_3$-350; d: $SnO_2@Al_2O_3$-60) prepared by using SnO_2 with various sizes, i.e., (a) ~1.6 μm, (b) ~600 nm, (c) ~350 nm, and (d) ~60 nm. (i–l) The corresponding scheme for the formation of $Sn@Al_2O_3$. All scale bars are 500 nm.

3.3 From Core-Shell to Yolk-Shell and Hollow: Controllable Nanostructure via Liquid Metal Diffusions

In this part (Chapter 4), Sn NPs were encapsulated with SiO_2 shell to form $Sn@SiO_2$ core-shell NPs, then loaded on a TEM holder with heating function and heated to 300°C in vacuum with in-situ TEM observation. It was observed that hollow NPs formed after heating. During real-time observation at 300°C, it was found that, under strong electron beam condition (37.3 $pA \cdot cm^{-2}$), Sn cores in $Sn@SiO_2$ move dynamically with deformation of encapsulating SiO_2 structure. The disappearance of liquid state Sn cores occurs in both strong (37.3 $pA \cdot cm^{-2}$) and weak (2.7 $pA \cdot cm^{-2}$) electron beam conditions, but in different modes. Combined above results with the observed Ostwald ripening inside SiO_2 during heating, it is believed that the diffusion of Sn occurs which contributes to the formation of hollow nanostructure.

With this understanding, controllable nanostructures from core-shell NPs to yolk-shell NPs and hollow NPs were synthesized by tuning the core-shell volumetric ratio of starting $Sn@SiO_2$ core-shell NPs with annealing in a sealed pan in a differential scanning calorimeter (DSC) in sequence. By measuring the volume of remained Sn core and the diameter of original Sn core from more than 200 yolk-shell and hollow NPs, it was found that the amorphous SiO_2 shell that fabricated in this case provides space with a certain capacity for Sn species to stay after heating and diffusion. The diffused Sn may interact with the dangling bonding in SiO_2, making the Sn stay as the state of SnO_x, and leaving hollow space in the center, thus creating the hollow structrue. The high-angle annular dark-field scanning transmission electron microscopy (HAADF-STEM) image and EDS mapping of obtained hollow NPs show that the Sn element was distributed inside the SiO_2 shell, giving evidence to the Sn diffusion.

4. Conclusion and Prospective

- A nanostructure in which phase-change Sn NPs were confined inside p-SiO_2 spheres was synthesized through a facile method utilizing common starting chemicals. The p-SiO_2 spheres effectively stabilized the embedded Sn NPs during cyclic melting–cooling. The melting depression phenomenon of the Sn NPs expands the application window of phase-change thermal energy storage using low-melting-temperature metals. The formation of voids inside Sn NPs@p-SiO_2 was investigated for the first time. The transformation of the Sn precursor occurred and included the formation and decomposition of the amorphous Sn precursor, formation and reduction of crystal Sn oxides, and interactions between Sn NPs and SiO_2 during annealing in a 3% H_2/N_2 atmosphere. It is believed that the transformation of the Sn precursor during annealing accompanied by the modification of the formed Sn NPs led to the formation of big voids inside p-SiO_2 spheres, which gives inspiration for new strategies for the synthesis of hollow SiO_2 spheres and yolk–shell SiO_2 structures.
- Alumina-encapsulated Sn particles ($Sn@Al_2O_3$) were successfully prepared and used as PCMs. The fabrication process consisted of a surfactant-free solvothermal synthesis of SnO_2spheres, boehmite treatment on SnO_2 spheres, calcination in the air, and the final

hydrogen reduction to transform SnO_2 to metallic Sn. All the steps of fabrication are facile and low-cost which can be simply applied to the mass production. The as-obtained $Sn@Al_2O_3$ particles with a high PCM content (92.37 wt %) showed a stable thermal behavior and morphology during 100 melt–freeze cycles in the air atmosphere. The $Sn@Al_2O_3$ shows a core–shell structure with small Sn nanoparticles dispersed in the shell. The formation of $Sn@Al_2O_3$ structure is a result of boehmite treatment on SnO_2spheres for the involvement of aluminum. The penetration of boehmite sol (AlOOH) into the SnO_2 spheres contributes to the formation of the thick alumina shell, which plays a key role in the thermal storage stability. This result also provided the possibility for a facile method for designing new metal nanoparticles with a particle-distributed nanostructure. These results also demonstrate the great potential of $Sn@Al_2O_3$ particles in the applications as a thermal energy storage material in high-temperature conditions which are not suitable for organic PCMs.

- A novel design of controllable nanostructure of $Sn@SiO_2$ from core-shell to yolk-shell and hollow has been achieved through a liquid metal diffusion process. The transformation of $Sn@SiO_2$ core-shell nanoparticles into hollow SiO_2 nanostructure by diffusion of liquid Sn cores inside $Sn@SiO_2$ was real-time observed via in-situ TEM. The diffusion of liquid state Sn acts as the role for removing the cores thus creating the cavity for hollow nanostructure. Importantly, based on these findings, the control over the morphologies of hollow/yolk-shell $Sn@SiO_2$ nanostructures was demonstrated by adjusting the volume ratio between core and shell of starting $Sn@SiO_2$ core-shell nanoparticle precursors. Furthermore, these findings provide valuable knowledge of diffusion of liquid state metal inside SiO_2 structure, as well as a novel tool in designing complicated hollow nanostructures in future studies.

References

1. Zhao, C. Y.; Zhang, G. H. Review on microencapsulated phase change materials (MEPCMs): Fabrication, characterization and applications. *Renew. Sust. Energ. Rev.* **2011,** *15* (8), 3813-3832.
2. Mohamed, S. A.; Al-Sulaiman, F. A.; Ibrahim, N. I.; Zahir, M. H.; Al-Ahmed, A.; Saidur, R.; Yılbaş, B. S.; Sahin, A. Z. A review on current status and challenges of inorganic phase change materials for thermal energy storage systems. *Renew. Sust. Energ. Rev.* **2017,** *70*, 1072-1089.
3. Pielichowska, K.; Pielichowski, K. Phase change materials for thermal energy storage. *Prog. Mater. Sci.* **2014,** *65*, 67-123.
4. Aftab, W.; Huang, X.; Wu, W.; Liang, Z.; Mahmood, A.; Zou, R. Nanoconfined phase change materials for thermal energy applications. *Energy Environ. Sci.* **2018,** *11* (6), 1392-1424.
5. Alam, T. E.; Dhau, J. S.; Goswami, D. Y.; Stefanakos, E. Macroencapsulation and characterization of phase change materials for latent heat thermal energy storage systems. *Appl. Energ.* **2015,** *154*, 92-101.
6. Liu, M.; Saman, W.; Bruno, F. Review on storage materials and thermal performance enhancement techniques for high temperature phase change thermal storage systems. *Renew. Sust. Energ. Rev.* **2012,** *16* (4), 2118-2132.

7. Ge, H.; Li, H.; Mei, S.; Liu, J. Low melting point liquid metal as a new class of phase change material: An emerging frontier in energy area. *Renew. Sust. Energ. Rev.* **2013,** *21*, 331-346.
8. Yang, X.-H.; Tan, S.-C.; He, Z.-Z.; Liu, J. Finned heat pipe assisted low melting point metal PCM heat sink against extremely high power thermal shock. *Energy Convers. Manag.* **2018,** *160*, 467-476.
9. Hering, W.; Stieglitz, R.; Wetzel, T. Application of liquid metals for solar energy systems. *EPJ Web of Conferences* **2012,** *33*, 03003.
10. Pacio, J.; Singer, C.; Wetzel, T.; Uhlig, R. Thermodynamic evaluation of liquid metals as heat transfer fluids in concentrated solar power plants. *Appl. Therm. Eng.* **2013,** *60* (1), 295-302.
11. Ge, H.; Liu, J. Phase change effect of low melting point metal for an automatic cooling of USB flash memory. *Front. Energy* **2012,** *6* (3), 207-209.
12. Lin, Y.; Cooper, C.; Wang, M.; Adams, J. J.; Genzer, J.; Dickey, M. D. Handwritten, Soft Circuit Boards and Antennas Using Liquid Metal Nanoparticles. *Small* **2015,** *11* (48), 6397-403.
13. Miner, A.; Ghoshal, U. Cooling of high-power-density microdevices using liquid metal coolants. *Appl. Phys. Lett.* **2004,** *85* (3), 506-508.
14. Ma, K.-Q.; Liu, J. Heat-driven liquid metal cooling device for the thermal management of a computer chip. *J. Phys. D: Appl. Phys.* **2007,** *40* (15), 4722-4729.
15. Ghadimi, A.; Saidur, R.; Metselaar, H. S. C. A review of nanofluid stability properties and characterization in stationary conditions. *Int. J. Heat Mass Transfer* **2011,** *54* (17), 4051-4068.
16. Muta, H.; Kurosaki, K.; Uno, M.; Yamanaka, S. Thermoelectric properties of constantan/spherical SiO_2 and Al_2O_3 particles composite. *J. Alloys Compd.* **2003,** *359* (1), 326-329.
17. Hsu, T.-H.; Chung, C.-H.; Chung, F.-J.; Chang, C.-C.; Lu, M.-C.; Chueh, Y.-L. Thermal hysteresis in phase-change materials: Encapsulated metal alloy core-shell microparticles. *Nano Energy* **2018,** *51*, 563-570.
18. Kravchyk, K.; Protesescu, L.; Bodnarchuk, M. I.; Krumeich, F.; Yarema, M.; Walter, M.; Guntlin, C.; Kovalenko, M. V. Monodisperse and Inorganically Capped Sn and Sn/SnO_2 Nanocrystals for High-Performance Li-Ion Battery Anodes. *J. Am. Chem. Soc.* **2013,** *135* (11), 4199-4202.